Organic Electronics 14 (2013) 1577–1585

Contents lists available at SciVerse ScienceDirect

Organic Electronics

journal homepage: www.elsevier.com/locate/orgel

Light trapping schemes in organic solar cells: A comparison between optical Tamm states and Fabry–Pérot cavity modes

Xu-Lin Zhang [a], Jun-Feng Song [a,b,*], Xian-Bin Li [a], Jing Feng [a], Hong-Bo Sun [a,c,*]

[a] State Key Laboratory on Integrated Optoelectronics, College of Electronic Science and Engineering, Jilin University, 2699 Qianjin Street, Changchun 130012, People's Republic of China
[b] Institute of Microelectronics, A*STAR (Agency for Science, Technology and Research), 11 Science Park Road, Singapore Science Park II, Singapore 117685, Singapore
[c] College of Physics, Jilin University, Changchun 130012, People's Republic of China

ARTICLE INFO

Article history:
Received 14 January 2013
Received in revised form 14 March 2013
Accepted 19 March 2013
Available online 4 April 2013

Keywords:
Organic solar cells
Light trappings
Optical Tamm states
Fabry–Pérot cavity modes

ABSTRACT

Recently optical Tamm states at metal/photonic crystals interface have been applied in thin-film organic solar cells (OSCs) as a new light trapping scheme for photon absorption enhancement. In this work, we theoretically investigate this scheme thoroughly to optimize the absorption performance for such optical Tamm states based OSCs (OTS–OSCs). We find that the overall absorptivity of the OTS–OSCs can be improved by using photonic crystals bilayers with a higher refractive index contrast, which is a result of the more strongly enhanced field intensity in the active layers. The conventional Fabry–Pérot cavity modes based OSCs (FP–OSCs) are also studied for comparison, whose absorption performance is found to be strongly dependent on the refractive index of the additional dielectric layer. These two schemes based OSCs exhibit comparable absorption performance in aspects of absorption enhancement, field distributions, and angle effect in the planar case. However, the proposed OTS–OSCs exhibit ~10% higher overall absorptivity than that for the FP–OSCs in the corrugated case, if both OSCs exhibit the same overall absorptivity in the planar case. The reduced absorption in the corrugated FP–OSCs is a result of the strong scatterings induced losses in the metal, which can be avoided by the photonic crystals bilayers in the OTS–OSCs. Therefore, the proposed Tamm states based scheme shows a higher value in corrugated OSCs.

1. Introduction

Organic solar cells (OSCs) are a promising approach for high-performance photovoltaics with low-cost, lightweight, and mechanical flexibility [1–3]. The most widely studied OSCs are conjugated polymer-based OSCs [4,5] and small molecules-based OSCs [6,7]. In small molecules-based OSCs, the active layers are required to be much thinner than 100 nm in view of the short diffusion length of excitons [8]. However, the incident photons could not be absorbed efficiently with such thin active layers. To overcome this obstacle, advanced light trapping schemes have been proposed. A well-known scheme is based on the Fabry–Pérot (FP) cavity modes oscillating between two metal reflectors. The optical absorption can be considerably enhanced if the FP resonant wavelength range matches well with the high-absorption range of the active layer [9]. Another scheme based on surface plasmon polaritons (SPPs) has also been investigated extensively [9–11]. Enhanced photon absorption can be achieved via the excitations of propagating SPPs and localized SPPs through the introductions of metallic gratings [6] and metallic nanoparticles [12] into the OSCs, respectively. In addition to the effect of diffractions, the metallic gratings and nanoparticles still ex-

* Corresponding authors at: State Key Laboratory on Integrated Optoelectronics, College of Electronic Science and Engineering, Jilin University, 2699 Qianjin Street, Changchun 130012, People's Republic of China. Tel./fax: +86 431 85168281 (H.-B. Sun).
E-mail addresses: songjf@ime.a-star.edu.sg (J.-F. Song), hbsun@jlu.edu.cn (H.-B. Sun).

1566-1199/$ - see front matter © 2013 Elsevier B.V. All rights reserved.
http://dx.doi.org/10.1016/j.orgel.2013.03.029

hibit an effect of strong scatterings [9]. Therefore, the SPPs based scheme is more effective for light trappings although at the cost of a requirement for manufacturing complicated micro-nanostructures [13].

Recently, optical Tamm states at metal/photonic crystals interface [14] have been applied to OSCs as a new light trapping scheme [15]. Such Tamm states are surface waves at metal/photonic crystals interface with local maximum field intensity at the surface. The field intensity of Tamm states decays into the photonic crystals due to the Bragg forbidden effect [14]. It has been shown in our previous work that the optical Tamm states scheme based OSCs (OTS–OSCs) exhibit considerable absorption enhancement for dual-polarized incidence as a result of the excitation of broadband Tamm states [15]. However, this new scheme has not been investigated thoroughly, and more details are needed to be studied to further improve the absorption performance in the OTS–OSCs. Moreover, a comparison between the new Tamm states based scheme and the conventional FP cavity modes based scheme is needed to evaluate their respective characteristics for light trappings, as they exhibit similar characteristics such as the absorption enhancement for dual-polarizations. Such comparison will be valuable for the practical choice of the light trapping scheme in experimental designs.

In this work, we investigate the OTS–OSCs to optimize the absorption performance. We find that a larger absorption enhancement can be achieved in an OTS–OSC with photonic crystals bilayers exhibiting a higher refractive index contrast. This is a result of the more strongly enhanced field intensity in the active layers. For comparison, the conventional FP cavity modes based OSCs (FP–OSCs) are also studied, whose absorption performance is found to be strongly dependent on the refractive index of the additional dielectric layer. We compare these two schemes based OSCs in planar and corrugated case, respectively. In the planar case, both OSCs exhibit comparable absorption performance in aspects of absorption enhancement, field distributions, and angle effect. In the corrugated case, the proposed OTS–OSCs exhibit ~10% higher overall absorptivity than that for the FP–OSCs, if both OSCs exhibit the same overall absorptivity in the planar case. The reduced absorption in the corrugated FP–OSCs is a result of the strong scatterings induced losses in the metal, which can be avoided by the photonic crystals bilayers in the OTS–OSCs. Therefore, the proposed Tamm states based scheme shows a higher value than the conventional FP cavity modes based scheme in corrugated OSCs.

2. Devices and simulation details

A schematic of the studied OSCs is shown in Fig. 1. Fig. 1a illustrates a reference OSC (R–OSC). This copper phthalocyanine–perylene tetracarboxylic bisbenzimidazole (CuPc–PTCBI) based thin-film OSC has been used as a model to investigate the SPPs based scheme for photon absorption enhancement in some previous literatures [10,11]. An opaque Ag film and a transparent poly(3,4-ethylenedioxythiophene) (PEDOT) layer are used as electrodes. In this study, the structure parameters are chosen the same as those in the aforementioned literatures. Fig. 1b shows our designed OTS–OSC with photonic crystals stacked outside the organic layers. The refractive index and thickness of the alternating layers are denoted by n_1, n_2, d_1, and d_2, respectively, while the number of photonic crystals bilayers is given by n_{PC}. To compare with the OTS–OSC, the FP–OSC is also studied in this work. The structure is shown in Fig. 1c, where a thin-film Ag with thickness d_4 is used as a reflector to support the FP cavity modes. As the total thickness of the organic layers is too thin (~47 nm), a dielectric layer (n_3, d_3) should be added for the formation of FP cavity modes within the high-absorption wavelength range of the active layers (600 nm ~ 700 nm) [10].

We apply in-house generated finite-difference time-domain (FDTD) codes [15–17] to calculate the absorptivity spectra in the active layers (CuPc and PTCBI) for the three types of OSCs. In the calculations, the refractive index and extinction coefficients of the organic layers are extracted from experimental measurements [6]. The Drude model is applied to deal with Ag in the FDTD simulations [16]. As the refractive index of CuPc and PTCBI are too complex that cannot be fitted into a Drude model, we need to deal with only one wavelength in one FDTD simulation. Although it will take much more rounds of simulations, the refractive index for the active layers and Ag can be as accurate as the experimental results providing different parameters of the Drude model are fitted and used for different wavelengths. More specifically, the Drude model for Ag can be written as $\varepsilon_{Ag} = 1 - \omega_p^2/(\omega^2 + i\omega\gamma)$, where ε_{Ag} is the permittivity for Ag, ω, ω_p, and γ are the frequency, plasma frequency, and plasma collision rate, respectively. The permittivity for Ag is shown in Fig. 1d, which is extracted from the RSoft package. For each frequency, a direct solution of the above Drude model is as follows: $\gamma = \mathrm{Im}(\varepsilon_{Ag})\omega/[1 - \mathrm{Re}(\varepsilon_{Ag})]$, $\omega_p^2 = \mathrm{Im}(\varepsilon_{Ag})(\omega^3 + \omega\gamma^2)/\gamma$, where $\mathrm{Re}(\varepsilon_{Ag})$ and $\mathrm{Im}(\varepsilon_{Ag})$ correspond to the real and imaginary parts of the permittivity for Ag, respectively. The calculated parameters of the Drude model for each wavelength are shown in Fig. 1e, through which the accuracy of the FDTD simulations can be guaranteed.

The TM (TE) total absorptivity A_{TM} (A_{TE}) and overall absorptivity A_{Total}, which are calculated by $A_{TM(TE)} = \frac{\int_{400\ nm}^{900\ nm} a_{TM(TE)}(\lambda)S(\lambda)d\lambda}{\int_{400\ nm}^{900\ nm} S(\lambda)d\lambda}$ and $A_{Total} = \frac{A_{TM}+A_{TE}}{2}$, are applied as criteria for the absorption performance of the OSCs [10,15]. In these equations, $a_{TM}(\lambda)$ and $a_{TE}(\lambda)$ are the absorptivity spectra in the active layers for TM- and TE-polarized incidence, respectively, and $S(\lambda)$ is the solar irradiance spectrum under AM1.5 illumination [10]. In Fig. 1, α indicates the incident angle of the plane wave.

3. Results and discussion

The materials in this section are organized as follows. We first investigate the absorption performance of the planar OTS–OSCs and FP–OSCs in Sections 3.1 and 3.2, respectively. Then we give a comparison of these two planar devices in Section 3.3. Finally, we study the two OSCs integrated with wavelength-scale periodic gratings to reveal the superiorities of the proposed OTS–OSCs in Section 3.4.

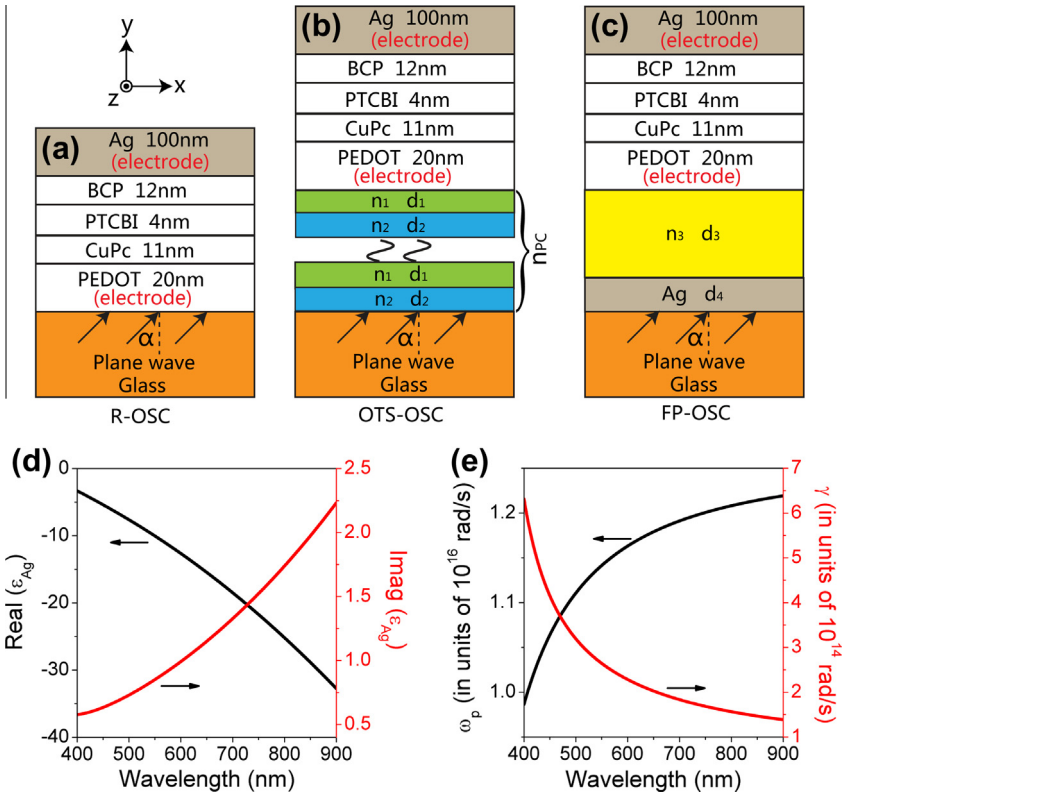

Fig. 1. Schematics of the (a) reference OSC (R–OSC), (b) Tamm states based OSC (OTS–OSC) and (c) FP cavity modes based OSC (FP–OSC). In the OTS–OSC, photonic crystals bilayers are stacked outside the organic layers for the excitation of Tamm states. In the FP–OSC, an additional dielectric and an added thin Ag layer are needed to support the FP cavity modes. In all these three figures, α indicates the incident angle of the plane wave. (d) The permittivity of Ag extracted from the RSoft package. (e) The fitted plasma frequency and plasma collision rate for the Drude model of Ag.

3.1. Absorption performance of planar OTS–OSCs

In this sub-section, we study the absorption performance of the planar OTS–OSCs shown in Fig. 1b. We will show that the overall absorptivity of the OTS–OSCs strongly depends on the number and refractive index contrast of the photonic crystals bilayers.

We first investigate the OTS–OSCs with different numbers of photonic crystals bilayers n_{PC}. The photonic crystals parameters are chosen as $n_1 = 1.5$, $n_2 = 2.2$, $d_1 = 130$ nm, and $d_2 = 82$ nm, respectively. Such refractive index can be achieved by introducing alternating layers of antimony-doped tin oxide (ATO) and tin-doped indium oxide (ITO) [18]. Once the refractive index of the photonic crystals bilayers are determined, such combinations of d_1 and d_2 are chosen that the Tamm states wavelength range optimally overlaps with the high-absorption range of the active layers [15]. More specifically, we have scanned different combinations of d_1 and d_2 until a maximum A_{Total} was obtained, while $n_1 = 1.5$, $n_2 = 2.2$, and $n_{PC} = 1$ were fixed. The absorptivity spectra in the active layers with $n_{PC} = 1$ (red dashed line), $n_{PC} = 2$ (blue dotted line), and $n_{PC} = 3$ (green dash-dotted line) are shown in Fig. 2a for TE-polarized normal incidence ($\alpha = 0°$). The result for the R–OSC is also given for comparison by the black solid line, where two intrinsic absorption peaks of CuPc located at 615 nm and 685 nm can be seen. Compared with the R–OSC, considerable absorption enhancement can be achieved in the OTS–OSCs via the excitation of Tamm states. The more photonic crystals bilayers are introduced, the stronger but narrower enhanced absorption peaks appear.

We focus on the OTS–OSC with $n_{PC} = 3$. The electric field (E_z) intensity $|E_z|$ profiles are shown in Fig. 2b. In the calculations, normal plane waves with unity electric amplitude intensity are used as the incidence. Therefore, the electric field intensity also indicates the field enhancement in comparison with the incidence. From the black dashed circle region, the excitation of a narrow band Tamm states around the wavelength of 685 nm is confirmed, with the fields exhibiting those oscillating–damping profiles into the photonic crystals [14]. The excitation of such Tamm states can induce a field enhancement in the active layers associated with an enhancement in the overall absorptivity. However, the bandwidth of the enhanced absorption peak is relatively narrow, whereas broadband absorption enhancement is always required in OSCs. We will show below that this can be achieved via using less photonic crystals bilayers.

The electric field intensity $|E_z|$ profiles for $n_{PC} = 1$ are shown in Fig. 2c. Compared with the field profiles for $n_{PC} = 3$ in Fig. 2b, a broader but weaker field enhancement can be observed. In order to judge which one is better for OSCs, the overall absorptivity A_{Total} is calculated as shown by the inset of Fig. 2a. The OTS–OSCs exhibit the overall

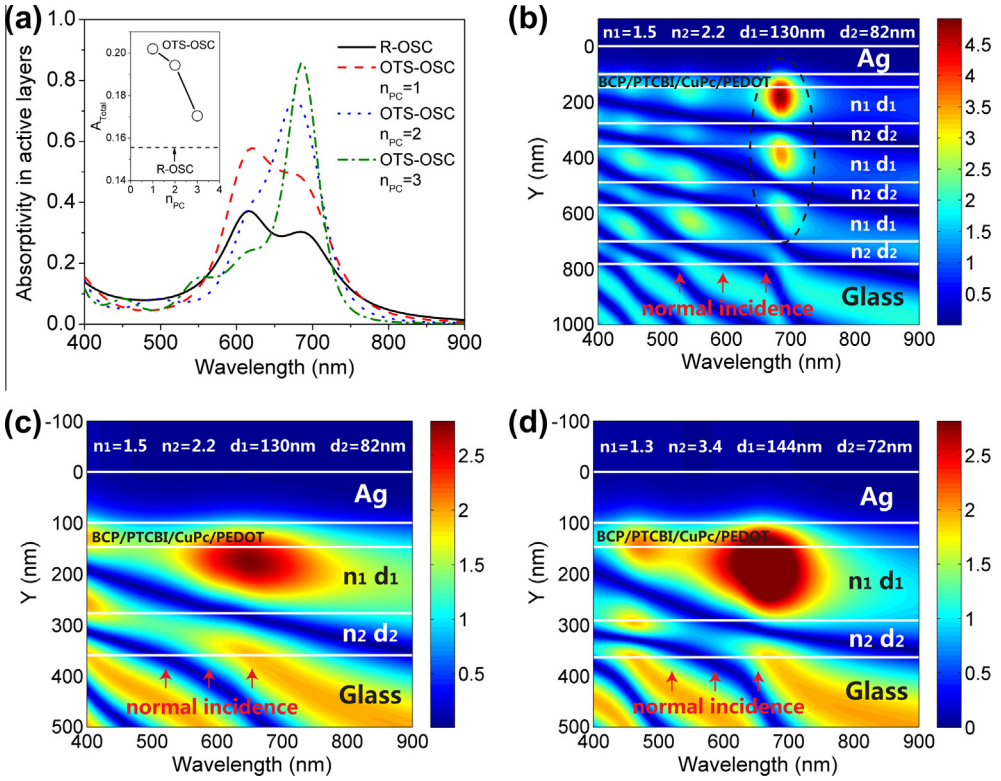

Fig. 2. (a) Absorptivity spectra in the active layers for the R–OSC (black solid line) and OTS–OSCs with $n_{PC} = 1$ (red dashed line), 2 (blue dotted line), and 3 (green dash-dotted line), respectively. The photonic crystals parameters of the OTS–OSCs are chosen as $n_1 = 1.5$, $n_2 = 2.2$, $d_1 = 130$ nm, and $d_2 = 82$ nm. The inset shows the overall absorptivity for these OSCs. (b–c) Electric field intensity $|E_z|$ profiles for the OTS–OSCs with (b) $n_{PC} = 3$ and (c) $n_{PC} = 1$. The photonic crystals parameters are chosen the same as those in (a). (d) Electric field intensity $|E_z|$ profiles for the OTS–OSC with $n_{PC} = 1$. The photonic crystals parameters are chosen as $n_1 = 1.3$, $n_2 = 3.4$, $d_1 = 144$ nm, and $d_2 = 72$ nm. For comparison, the color bars are chosen the same for (c) and (d). In all these figures, we study the planar OSCs with normal TE-polarized incidence (For interpretation of the references to color in this figure legend, the reader is referred to the web version of this article.).

absorptivity of 0.202, 0.194, and 0.171 for cases of $n_{PC} = 1$, 2, and 3, which is 29%, 24%, and 10% higher than that of the R–OSC (~0.156), respectively. Therefore, less photonic crystals bilayers are preferred in OTS–OSCs, which is a result of the requirement for broadband absorption enhancement in OSCs. Although one bilayer cannot be called as photonic crystals, the reflection property from such one bilayer in the forbidden band can still be comparable to that from a ~10 nm-thick Ag layer. We will show in Section 3.2 that the best performance of the FP–OSC can be achieved with an added Ag layer of ~10 nm in thickness. It is familiar to us that the mode between an opaque Ag layer and a ~10 nm-thick Ag layer can be called as a FP cavity mode. In analogy with the FP cavity modes, we therefore decide to call the states between an opaque Ag layer and one photonic crystal bilayer as optical Tamm states as well. These optical Tamm states and FP cavity modes are weakly bounded but broadband, which benefit the OSCs due to the requirement of broadband absorption.

We then consider the effect of the refractive index of the photonic crystals bilayers on the absorptivity enhancement. In this work, the absorptivity enhancement is defined as a ratio of the overall absorptivity for the OTS–OSC (or FP–OSC) to that for the R–OSC. It is calculated as a function of n_2 as shown by the black-circle line in Fig. 3a, where $n_1 = 1.5$ and $n_{PC} = 1$ are kept unchanged. We observe that the absorptivity enhancement becomes larger with the increase in n_2. It should be noted that the choices of d_1 and d_2 depend on the refractive index of the photonic crystals bilayers. It can be found in Fig. 3a that a decreasing combination of d_1 (red-square line) and d_2 (red-triangle line) should be chosen with the increase of n_2 in order to obtain a maximum value of A_{Total}. This adjustment of the layer thicknesses comes from the fact that the Tamm states wavelength range should always have maximum overlap with the high-absorption range of the active layers.

Fig. 3b shows the absorptivity enhancement as a function of n_2 while $n_1 = 1.3$ and $n_{PC} = 1$ are chosen (black-square line). We observe that such OTS–OSCs exhibit a larger absorptivity enhancement than that in the devices with $n_1 = 1.5$ and $n_{PC} = 1$ (black-circle line). Therefore, we state that a larger absorptivity enhancement can be achieved in an OTS–OSC with photonic crystals bilayers exhibiting a higher refractive index contrast. In the inset of Fig. 3b, the absorptivity spectra in the active layers for two OTS–OSCs, one with $n_1 = 1.5$ and $n_2 = 2.2$ (red-dashed line), and the other with $n_1 = 1.3$ and $n_2 = 3.4$ (blue-dotted line), are shown for comparison. It is noted that the device with a higher refractive index contrast exhibits a better absorption

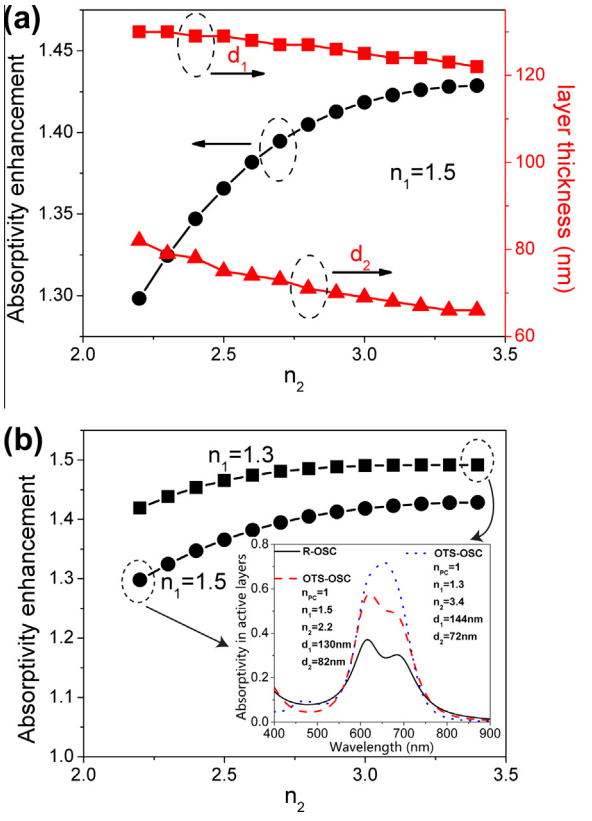

Fig. 3. (a) Absorptivity enhancement (black-circle line) for the OTS–OSCs as a function of n_2 associated with the corresponding choice of d_1 (red-square line) and d_2 (red-triangle line), where n_1 is fixed as 1.5. (b) Absorptivity enhancement as a function of n_2 for the OTS–OSCs with $n_1 = 1.5$ (black-circle line) and $n_1 = 1.3$ (black-square line). The inset shows a comparison on the absorptivity spectra between two OTS–OSCs marked by the dashed circles. The structure parameters are also indicated in the inset. In all these figures, we study the planar OSCs with $n_{PC} = 1$ (For interpretation of the references to color in this figure legend, the reader is referred to the web version of this article.).

performance. Here we give an explanation for this phenomenon from the field point of view. Fig. 2d shows the electric field intensity $|E_z|$ profiles for the OTS–OSC with $n_1 = 1.3$ and $n_2 = 3.4$, where the color bar is set the same as that in Fig. 2c. Compared with the field profiles in Fig. 2c ($n_1 = 1.5$ and $n_2 = 2.2$), a larger field enhancement can be observed in the active layers. Such enhanced field intensity can induce a larger overall absorptivity. Therefore, it can be concluded that a larger overall absorptivity can be obtained in the OTS–OSC with the photonic crystal bilayers exhibiting a higher refractive index contrast. The overall absorptivity for the OTS–OSC shown in Fig. 2d is as high as 0.232, which is ~49% higher than that for the R–OSC. Such excellent absorption performance in the case of normal incidence approaches the one (~50% enhancement) achieved via introducing metallic gratings for the excitation of SPPs [10]. This indicates the superiority of the proposed easily-manufactured OTS–OSCs, in which the absorption can be enhanced for both polarized incidence, whereas the absorption can be enhanced for only the TM-polarized incidence in those SPPs based OSCs [10,11].

3.2. Absorption performance of planar FP–OSCs

In this sub-section, we study the absorption performance of the FP–OSCs. We will show that the overall absorptivity of the FP–OSCs strongly depends on the refractive index of the additional dielectric layer.

We investigate the FP–OSCs with different refractive index of the additional dielectric layer. With a given n_3, the thicknesses of the additional dielectric layer d_3 and the added Ag layer d_4 have been scanned to find a maximum A_{Total}. We focus on the first-order FP cavity modes in this work. Fig. 4a shows the normal incidence TE-polarized absorptivity spectra in the active layers for the FP–OSCs with $n_3 = 2.2$, 1.3, and 1, respectively. The corresponding choices of d_3 and d_4 can be found in the figure. We observe that considerable absorption enhancement can be achieved for the FP–OSCs in comparison with that for the R–OSC due to the excitations of FP cavity modes.

The absorptivity enhancement as a function of n_3 for these FP–OSCs is shown in Fig. 4b by the black-circle line. The corresponding choices of d_3 and d_4 are also indicated by the red-square line and red-triangle line, respectively. It is obvious that a thinner additional dielectric layer is needed if its refractive index is higher. Meanwhile, the requirement for d_4 is slightly different. Interestingly, we observe that the FP–OSC with a lower n_3 exhibits a larger absorptivity enhancement. This can also be explained from the field point of view. In Fig. 4c and d, we show the electric field intensity $|E_z|$ profiles for cases of $n_3 = 2.2$ and 1.3, respectively, where the color bars are set the same. We find that the FP–OSC with a lower n_3 exhibits a larger field enhancement in the active layers. Therefore, such device has a larger absorptivity enhancement. The overall absorptivity for this FP–OSC is ~0.227, which is 46% higher than that for the R–OSC. This excellent absorption performance in the case of normal incidence also approaches that in the SPPs based OSCs [10].

3.3. Comparison between planar OTS–OSCs and FP–OSCs

We have investigated the absorption enhancement in planar OSCs via the excitations of Tamm states and FP cavity modes in the previous two sub-sections. In this sub-section, we give a comparison between these two schemes.

We first discuss their differentia, which mainly lies in the structure configurations and intrinsic physics. In OTS–OSCs, less photonic crystals bilayers with higher refractive index contrast are required to achieve broadband Tamm states in the devices. In FP–OSCs, an additional dielectric layer with lower refractive index and a thin metal reflector are needed to realize a stronger FP resonance in the devices. Physically, the Tamm states can be considered as resonant modes without cavities, such as those at metal/ photonic crystals interfaces [14]. It should be noted that although some organic layers exist between the Ag layer and the photonic crystals in the OTS–OSCs (Fig. 1b), their total thicknesses are only ~47 nm, which are not thick enough to support a first-order cavity mode in the wavelength range around 685 nm (the peak wavelength for $n_{PC} = 3$ in Fig. 2a). Therefore, the Tamm states in these thin-film OTS–OSCs can be considered as the zero-order

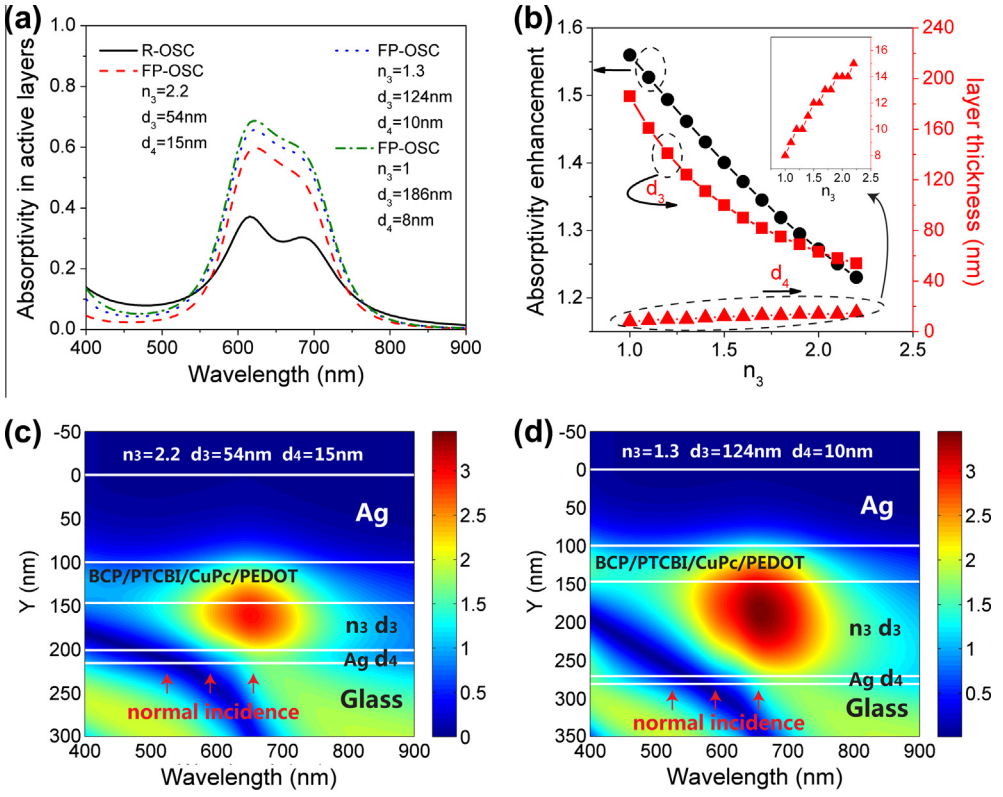

Fig. 4. (a) Absorptivity spectra in the active layers for the R–OSC (black solid line) and FP–OSCs with $n_3 = 2.2$ (red dashed line), 1.3 (blue dotted line), and 1 (green dash-dotted line), respectively. (b) Absorptivity enhancement (black-circle line) for the FP–OSCs as a function of n_3 associated with the corresponding choice of d_3 (red-square line) and d_4 (red-triangle line). (c–d) Electric field intensity $|E_z|$ profiles for the FP–OSCs with (c) $n_3 = 2.2$ and (d) $n_3 = 1.3$. For comparison, the color bars are chosen the same for (c) and (d). In all these figures, we study the planar OSCs with normal TE-polarized incidence (For interpretation of the references to color in this figure legend, the reader is referred to the web version of this article.).

cavity modes, whereas the FP cavity modes excited in the FP–OSCs are the first-order cavity modes.

Then we discuss the similarities of the two types of OSCs. Both the Tamm states and the FP cavity modes can be excited in planar devices, whereas the SPPs need to be excited with the assistance of metallic gratings or metallic nanoparticles. Moreover, both the OTS–OSCs and the FP–OSCs exhibit absorption enhancement for dual-polarized incidence, whereas the SPPs based OSCs exhibit absorption enhancement for only the TM-polarized incidence. These superiorities bring about those aforementioned planar OTS–OSCs and FP–OSCs with excellent absorption performance in the case of normal incidence which can be comparable to that of the SPPs based OSCs. Besides, the OTS–OSCs and FP–OSCs exhibit comparable enhanced absorptivity spectra (see the inset of Figs. 3b and 4a) and electric field intensity profiles (see Figs. 2c–d and 4c–d). The photonic crystals in the OTS–OSCs and the added Ag layer in the FP–OSCs are both used as reflectors. In consideration of broadband modes, less photonic crystals bilayers ($n_{PC} = 1$) and thinner added Ag layers (around 10 nm) should be chosen.

More similarities can be found by investigating the effect of the incident angle α on the absorption performance of the OSCs. The results are shown in Fig. 5a–c for the R–OSC, OTS–OSC, and FP–OSC, respectively. The structure parameters are shown in each figure. We observe that the overall absorptivity for the OTS–OSC and FP–OSC decreases dramatically with the increase in α. This is a result of the mismatching between the wavelength range of the cavity modes and the high-absorption range of the active layers. On the contrary, the deterioration of the overall absorptivity is not severe with increasing α for the R–OSC as no modes are supported in this device. Moreover, such dramatic decrease of the overall absorptivity is not observed in SPPs based OSCs [10]. This is due to the fact that the bandwidth of the SPPs modes is much broader than that of the cavity modes, and the SPPs can be excited for a wide range of angles of incidence.

3.4. Comparison between corrugated OTS–OSCs and FP–OSCs

We have concluded that the proposed planar OTS–OSCs exhibit comparable absorption performance to that of the conventional planar FP–OSCs. In this sub-section, we will show that corrugated OTS–OSCs exhibit a better absorption performance than that of corrugated FP–OSCs.

We have shown in our previous work [19] that FP cavity modes and SPPs can be cross-coupled to improve the performance of organic light-emitting devices. Applying the same idea here, we investigate corrugated OTS–OSCs and

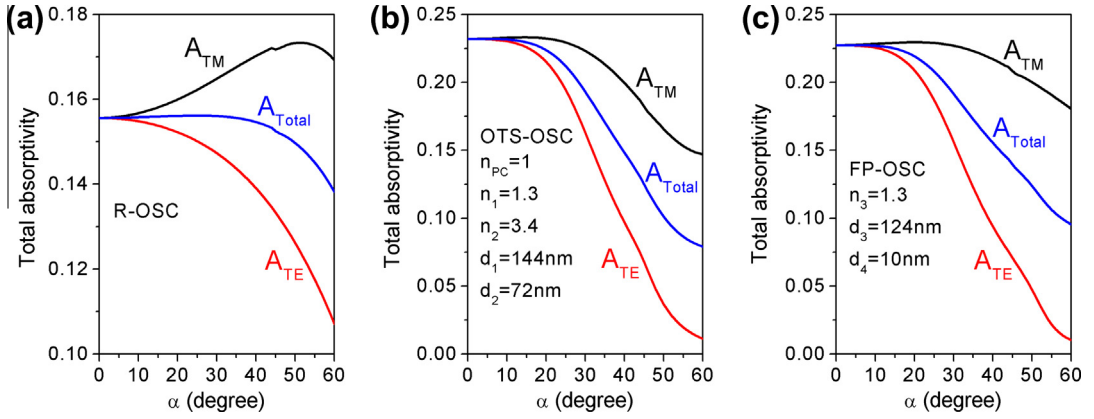

Fig. 5. TM total absorptivity (black line), TE total absorptivity (red line) and overall absorptivity (blue line) as a function of the incident angle α for the planar (a) R–OSC, (b) OTS–OSC, and (c) FP–OSC, respectively. The detailed structure parameters are indicated in each figure (For interpretation of the references to color in this figure legend, the reader is referred to the web version of this article.).

FP–OSCs integrated with one-dimensional 40 nm-height gratings to further improve the absorption performance. The profiles of such corrugated devices are illustrated in Fig. 6e and f. We consider an OTS–OSC with parameters of $n_{PC} = 1$, $n_1 = 1.5$, $n_2 = 2.2$, $d_1 = 130$ nm, and $d_2 = 82$ nm. For comparison, a FP–OSC with parameters of $n_3 = 1.9$, $d_3 = 64$ nm, and $d_4 = 10$ nm is also studied. As previously, the parameters of these two OSCs are optimized, and they exhibit the same overall absorptivity in the planar case. This can be confirmed from Fig. 6a and b for TM and TE polarization, respectively, where the black solid line, red dashed line, and blue dotted line show the absorptivity spectra for the planar R–OSC, OTS–OSC, and FP–OSC, respectively. In this sub-section, we only consider the cases of normal incidence.

Then we study these OSCs with 300 nm-period gratings. The aforementioned optimal structure parameters are also valid in the corrugated case, as the grating height (~40 nm) is much smaller than the period, which means the introducing of gratings may not affect the cavity modes too much [19]. Simulated absorptivity spectra for these corrugated OSCs are shown by the symbol-lines in Fig. 6a and b for TM and TE polarization, respectively. For TM polarization, SPPs peaks at ~540 nm (black dashed circle) for the three corrugated OSCs can be observed associated with broadband absorption enhancement compared with the planar ones. The magnetic field (H_z) intensity $|H_z|$ profiles for the corrugated OTS–OSC are shown in Fig. 6e. We find that propagating SPPs at the Ag/organic layers interface are excited associated with enhanced field intensity in the active layers.

Distinctions turn up at a longer wavelength range around 685 nm (black dotted circle) in Fig. 6a. The magnetic field intensity $|H_z|$ profiles at this wavelength for the corrugated OTS–OSC are shown in Fig. 6f. We observe that both strong scatterings at the metal electrode and Tamm states exist associated with enhanced absorption in the active layers. However, the absorptivity at this wavelength range (~685 nm) for the corrugated FP–OSC is much lower, which is nearly the same as that for the corrugated R–OSC. To explain this distinction, we calculate the distributions of all loss channels in the corrugated OTS–OSC and FP–OSC for TM polarization. The results are shown in Fig. 6c and d, where the red, yellow, and orange regions represent the absorption in the active layers, the losses in the Ag electrode, and the losses in the added Ag layer, respectively. We observe that more losses are dissipated in Ag for the corrugated FP–OSC, which is a result of the strong scatterings induced absorption in the added 10 nm-thick Ag. Such scatterings induced losses would limit the absorption in the active layers for the corrugated FP–OSC. On the contrary, the scatterings of the photonic crystals are not so strong and no losses would be dissipated in the photonic crystals for the corrugated OTS–OSC. Therefore, the corrugated OTS–OSC exhibits a larger TM total absorptivity than that of the FP–OSC.

For TE polarization shown in Fig. 6b, we find that the absorption performance for the corrugated devices is nearly the same as that for the planar ones, as SPPs could not be excited. In consideration of both polarizations, we conclude that the corrugated OTS–OSC exhibits a ~10% higher overall absorptivity than that of the FP–OSC, although both OSCs exhibit the same overall absorptivity in the planar case.

Finally, we show the calculated A_{TM}, A_{TE}, and A_{Total} for the three types of corrugated OSCs with various grating periods in Fig. 7. The black-, red-, and blue-symbol lines represent the results for the R–OSCs, OTS–OSCs, and FP–OSCs, respectively. The square-, triangle-, and circle-lines show the results for A_{TM}, A_{TE}, and A_{Total}, respectively. On one hand, the TM total absorptivity for the corrugated OTS–OSCs is larger than that for the corrugated FP–OSCs in each choice of period. The strong scatterings induced losses in the added Ag layer are the main reason for the reduced absorption in the FP–OSCs. On the other hand, the TE total absorptivity for the corrugated OTS–OSCs is comparable to that for the corrugated FP–OSCs, except the one with the period of 350 nm. This exception is due to the excitation of unexpected waveguide modes in the OTS–OSC [15], which should be avoided by choosing other appropriate grating

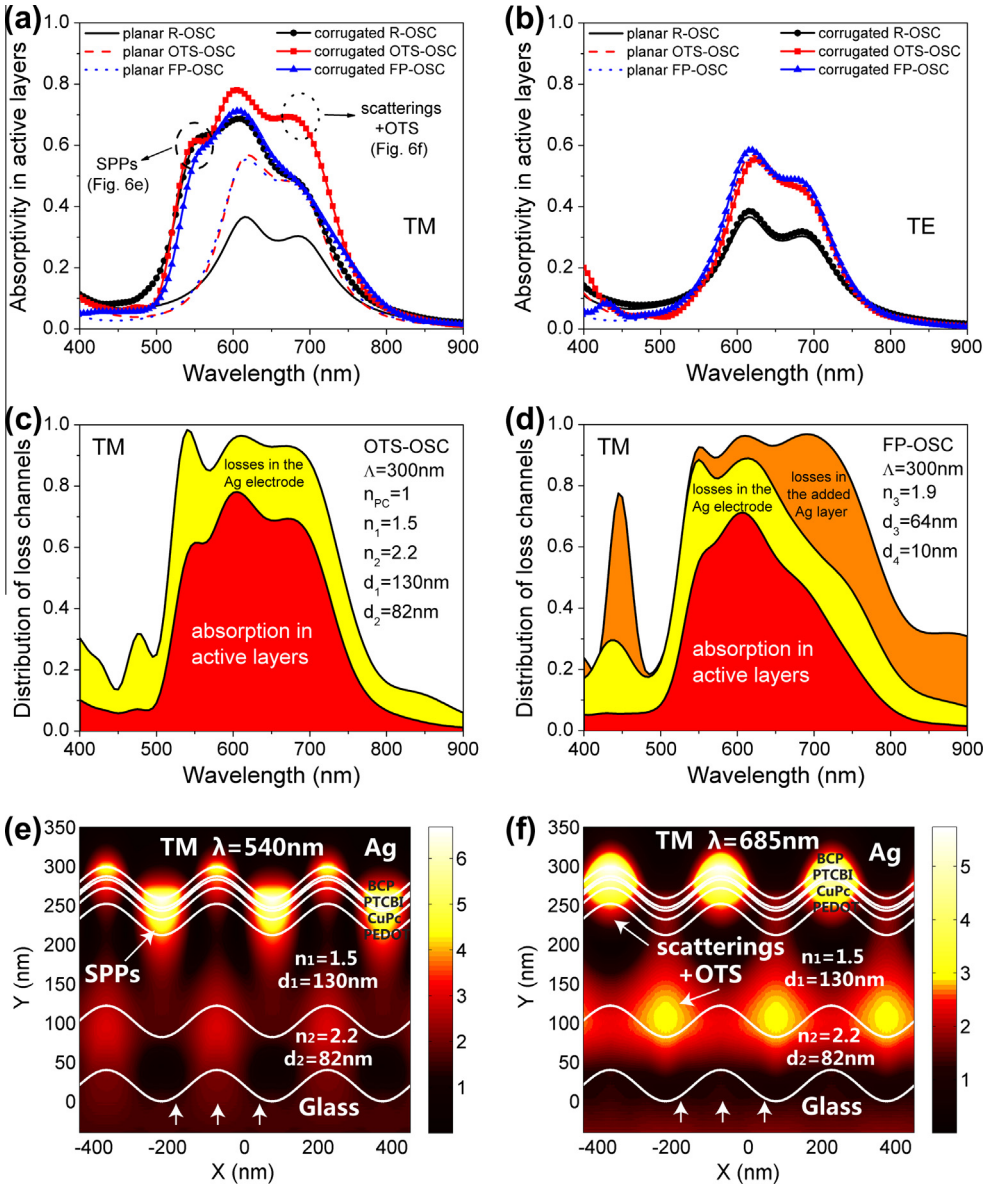

Fig. 6. (a and b) Absorptivity spectra in the active layers for planar R–OSC (black solid line), OTS–OSC (red dashed line), FP–OSC (blue dotted line), and corrugated R–OSC (black-circle line), OTS–OSC (red-square line), FP–OSC (blue-triangle line) with a period of 300 nm for normal (a) TM- and (b) TE-polarized incidence, respectively. (c and d) Distribution of all loss channels for the corrugated (c) OTS–OSC and (d) FP–OSC with a period of 300 nm for normal TM-polarized incidence. The red, yellow, and orange regions represent the absorption in the active layers, the losses in the Ag electrode, and the losses in the added Ag layer, respectively. (e and f) TM-polarized magnetic field intensity $|H_z|$ profiles for the corrugated OTS–OSCs with wavelengths of (e) 540 nm and (f) 685 nm, respectively. In all these figures, the structure parameters for the OTS–OSCs and FP–OSCs are chosen as $n_{PC} = 1$, $n_1 = 1.5$, $n_2 = 2.2$, $d_1 = 130$ nm, $d_2 = 82$ nm, $n_3 = 1.9$, $d_3 = 64$ nm, and $d_4 = 10$ nm (For interpretation of the references to color in this figure legend, the reader is referred to the web version of this article.).

periods. In consideration of both polarizations, the OTS–OSCs show superiorities for a larger overall absorptivity than the FP–OSCs in each choice of period. This indicates that the Tamm states based scheme is more appropriated for applications in corrugated OSCs. More specifically, the overall absorptivity of the corrugated OTS–OSC with a period of 300 nm is as high as 0.274, which is 78% and 10% higher than that of the planar R–OSC and the corrugated FP–OSC with the same grating period. Such excellent absorption performance in the case of normal incidence exceeds the one (~67% enhancement) achieved by using volumetric plasmonic resonator architectures [11] due to the excitations of both Tamm states and SPPs. The absorption performance of this corrugated OTS–OSC may be further improved by using photonic crystals bilayers with a higher refractive index contrast.

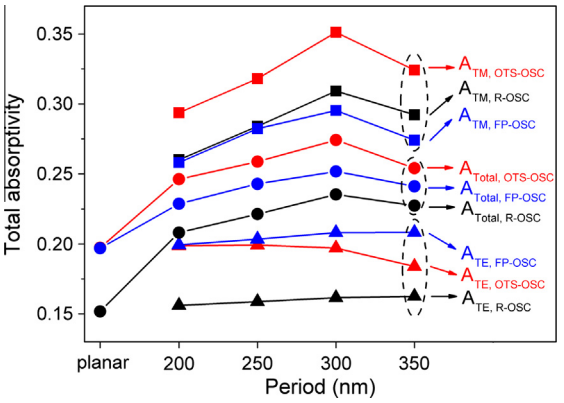

Fig. 7. TM total absorptivity (square line), TE total absorptivity (triangle line) and overall absorptivity (circle line) for the planar and corrugated R–OSCs (black line), OTS–OSCs (red line), and FP–OSCs (blue line) with various grating periods, respectively (For interpretation of the references to color in this figure legend, the reader is referred to the web version of this article.).

4. Conclusions

In summary, we have compared the light trapping schemes based on Tamm states and Fabry–Pérot cavity modes in planar and corrugated organic solar cells, respectively. In optical Tamm states based organic solar cells, a better absorption performance can be achieved by using photonic crystals bilayers with a higher refractive index contrast, which is a result of the more strongly enhanced field intensity in the active layers. In Fabry–Pérot modes based organic solar cells, a larger overall absorptivity can be obtained by using an additional dielectric layer with a lower refractive index. These two schemes based organic solar cells exhibit comparable absorption performance in aspects of absorption enhancement, field distributions, and angle effect in the planar case. However, the proposed optical Tamm states based organic solar cells show a better absorption performance than that for the Fabry–Pérot modes based organic solar cells in the corrugated case. The reduced absorption in the corrugated latter ones is a result of the strong scatterings induced losses in the metal, which can be avoided by the photonic crystals bilayers. Therefore, the proposed Tamm states based scheme shows a higher value in corrugated organic solar cells.

Acknowledgements

The authors gratefully acknowledge the financial support from NSFC (Grant Nos. 90923037, 61137001, 61107024, and 61177090).

References

[1] E. Avnon, N.Y. Gross, E. Ploshnik, R. Shenhar, N. Tessler, Low cost, nanometer scale nanoimprinting-application to organic solar cells optimization, Org. Electron. 12 (2011) 1241–1246.
[2] G. Li, V. Shrotriya, J. Huang, Y. Yao, T. Moriarty, K. Emery, Y. Yang, High-efficiency solution processable polymer photovoltaic cells by self-organization of polymer blends, Nat. Mater. 4 (2005) 864–868.
[3] Y.F. Liu, J. Feng, H.F. Cui, D. Yin, J.F. Song, Q.D. Chen, H.B. Sun, Highly flexible inverted organic solar cells with improved performance by using an ultrasmooth Ag cathode, Appl. Phys. Lett. 101 (2012) 133303.1–133303.4.
[4] C. Girotto, D. Cheyns, T. Aernouts, F. Banishoeib, L. Lutsen, T.J. Cleij, D. Vanderzande, J. Genoe, J. Poortmans, P. Heremans, Bulk heterojunction organic solar cells based on soluble poly(thienylene vinylene) derivatives, Org. Electron. 9 (2008) 740–746.
[5] Y. Zhou, H. Cheun, S. Choi, C.F. Hernandez, B. Kippelen, Optimization of a polymer top electrode for inverted semitransparent organic solar cells, Org. Electron. 12 (2011) 827–831.
[6] Y. Jin, J. Feng, X.L. Zhang, M. Xu, Y.G. Bi, Q.D. Chen, H.Y. Wang, H.B. Sun, Surface-plasmon enhanced absorption in organic solar cells by employing a periodically corrugated metallic electrode, Appl. Phys. Lett. 101 (2012) 163303.1–163303.4.
[7] H.W. Lin, H.W. Kang, Z.Y. Huang, C.W. Chen, Y.H. Chen, L.Y. Lin, F. Lin, K.T. Wong, An effective bilayer cathode buffer for highly efficient small molecule organic solar cells, Org. Electron. 13 (2012) 1925–1929.
[8] M. Agrawal, P. Peumans, Broadband optical absorption enhancement through coherent light trapping in thin-film photovoltaic cells, Opt. Exp. 16 (2008) 5385–5396.
[9] H.A. Atwater, A. Polman, Plasmonics for improved photovoltaic devices, Nat. Mater. 9 (2010) 205–213.
[10] C. Min, J. Li, G. Veronis, J.Y. Lee, S. Fan, P. Peumans, Enhancement of optical absorption in thin-film organic solar cells through the excitation of plasmonic modes in metallic gratings, Appl. Phys. Lett. 96 (2010) 133302.1–133302.3.
[11] M.A. Sefunc, A.K. Okyay, H.V. Demir, Volumetric plasmonic resonator architecture for thin-film solar cells, Appl. Phys. Lett. 98 (2011) 093117.1–093117.3.
[12] Y.H. Su, Y.F. Ke, S.L. Cai, Q.Y. Yao, Surface plasmon resonance of layer-by-layer gold nanoparticles induced photoelectric current in environmentally–friendly plasmon-sensitized solar cell, Light Sci. Appl. 1 (2012) e14.
[13] W. Xiong, Y.S. Zhou, X.N. He, Y. Gao, M.M. Samani, L. Jiang, T. Baldacchini, Y.F. Lu, Simultaneous additive and subtractive three-dimensional nanofabrication using integrated two-photon polymerization and multiphoton ablation, Light Sci. Appl. 1 (2012) e6.
[14] M. Kaliteevski, I. Irosh, S. Brand, R.A. Abram, J.M. Chamberlain, A.V. Kavokin, I.A. Shelykh, Tamm plasmon-polaritons: Possible electromagnetic states at the interface of a metal and a dielectric Bragg mirror, Phys. Rev. B 76 (2007) 165415.1–165415.5.
[15] X.L. Zhang, J.F. Song, X.B. Li, J. Feng, H.B. Sun, Optical Tamm states enhanced broad-band absorption of organic solar cells, Appl. Phys. Lett. 101 (2012) 243901.1–243901.5.
[16] X.L. Zhang, J. Feng, J.F. Song, X.B. Li, H.B. Sun, Grating amplitude effect on electroluminescence enhancement of corrugated organic light-emitting devices, Opt. Lett. 36 (2011) 3915–3917.
[17] X.L. Zhang, J.F. Song, X.B. Li, H.B. Sun, FDTD study on the invisibility performance of two-dimensional cylindrical cloak with off-plane incidence, IEEE J. Lightw. Technol. 30 (2012) 1835–1842.
[18] D.P. Puzzo, M.G. Helander, P.G. O'Brien, Z.B. Wang, N. Soheilnia, N. Kherani, Z.H. Lu, G.A. Ozin, Organic light-emitting diode microcavities from transparent conducting metal oxide photonic crystals, Nano Lett. 11 (2011) 1457–1462.
[19] Y. Jin, J. Feng, X.L. Zhang, Y.G. Bi, Y. Bai, L. Chen, T. Lan, Y.F. Liu, Q.D. Chen, H.B. Sun, Solving efficiency-stability tradeoff in top-emitting organic light-emitting devices by employing periodically corrugated metallic cathode, Adv. Mater. 24 (2012) 1187–1191.